JOURNAL OF GUIDANCE, CONTROL, AND DYNAMICS
Vol. 31, No. 3, May–June 2008

Multiple Method 2-D Trajectory Optimization Satisfying Waypoints and No-Fly Zone Constraints

Timothy R. Jorris* and Richard G. Cobb†
Air Force Institute of Technology, Wright–Patterson AFB, Ohio 45433

DOI: 10.2514/1.32354

Minimum time to target is one of the primary goals of a global strike mission. The Hypersonic Cruise Vehicle and the Common Aero Vehicle are currently being investigated for mission effectiveness. Additional mission requirements include passage through intermediate waypoints and avoidance of no-fly zones. Thus, a real-time or near real-time autonomous trajectory generation technique is desired to minimize the flight time, satisfy terminal and multiple intermediate state constraints, and remain within specified control limitations. The research herein presents a baseline technique, an analytical geometric trajectory optimization technique, and a dynamic optimization technique. Numerical examples for constant speed trajectories as well as decelerating flight are used to demonstrate and compare the presented techniques. These results show the significant time savings achievable through optimization, the accuracy and computation efficiency of the geometric solution, and the robustness and application of the dynamic optimization technique.

Nomenclature

a, a_c	=	acceleration, centripetal acceleration
C	=	control constraint
C_L, C_D	=	coefficient of lift, drag
d_1, d_2	=	distances from endpoint and turn radius
g_0	=	reference gravity, $g = g_0$ for constant altitude
H	=	Hamiltonian
J	=	cost function
k	=	fraction waypoint passage occurs along turn
L	=	integrand cost
M	=	no-fly zone interior state constraint
M_f	=	final Mach number
m	=	mass
N	=	waypoint interior state constraint
P_1, P_2	=	fixed endpoints
R	=	turn radius, or no-fly zone radius when subscripted
r_0	=	reference radius
S	=	no-fly zone constraint
T	=	leg time, that is, the time between two points
t	=	nondimensional time, a particular time when subscripted
u	=	normalized bank control $-1 \leq u \leq 1$
V	=	nondimensional speed
W_p	=	intermediate waypoint
x, y	=	states, coordinates when subscripted
$\mathbf{x}$	=	state vector
Δx, Δy	=	displacement from no-fly zone center
$\Delta\theta$	=	change in heading angle
θ	=	heading angle
λ	=	costate vector
μ_C	=	multiplier to adjoin the control constraint (C)
μ_S	=	multiplier to adjoin the no-fly zone constraint (S)
π_m	=	costate jump entering no-fly zone
π_n	=	costate jump at waypoint passage
σ	=	bank angle
Φ	=	adjoined terminal cost and constraint
ϕ	=	final state cost
χ	=	angle from waypoint to turn radius center
ψ	=	final state constraint

Subscripts

$C1$, $C2$	=	components of the μ_C vector
cj	=	center of no-fly zone j
f	=	final condition
i	=	waypoint number, passage of waypoint
j	=	no-fly zone number, entry to no-fly zone boundary
max	=	specified maximum
min	=	minimum acceptable
$m0$, $m1$	=	components of π_m vector
nx, ny	=	components of π_n vector
si	=	start of turn for waypoint i
u	=	partial derivative with respect to control u
w	=	waypoint passage
$\mathbf{x}$	=	partial derivative with respect to the state vector $\mathbf{x}$
x, y, V, θ	=	associated with respective state
0	=	initial condition

Superscripts

(1), (2), $(q-1)$, q	=	order of the time derivative
*	=	optimal
+	=	occurring just after, going forward in time
−	=	occurring just prior, going forward in time

Presented at the AAS/AIAA Spaceflight Mechanics Meeting, Sedona, Arizona, 28 January–1 February 2007; received 25 May 2007; revision received 26 September 2007; accepted for publication 27 September 2007.

*Ph.D. Graduate, Department of Aeronautics and Astronautics, 2950 Hobson Way, Building 640; timothy.jorris@us.af.mil. Member AIAA.

†Assistant Professor, Department of Aeronautics and Astronautics, 2950 Hobson Way, Building 640; richard.cobb@afit.edu. Senior Member AIAA.

I. Introduction

GLOBAL Strike (GS) and Global Persistent Attack (GPA) are two of the seven United States Air Force Concepts of Operations [1]. The Common Aero Vehicle (CAV) is an unmanned aerial vehicle (UAV) that could support these hypersonic reentry objectives. The CAV is also one possible payload aboard the

Hypersonic Cruise Vehicle. Additional requirements for this mission may include intermediate waypoints [2–7] which are specified for reconnaissance targets, no-fly zones which are specified for geopolitical restraints or threat avoidance [8–14], and a final target which is specified as the mission objective. Previous research in this area can be summarized as follows. Erzberger and Lee and Shapira and Ben-Asher in [2,3] compute optimal turn performance, whereas Innocenti et al., Whang and Whang, Moon and Kim, and Yang and Zhao in [4–7] specifically address intermediate waypoints. Bortoff and Judd and McLain in [9,10] construct a Voronoi diagram to partition threats, Kumar and Ghose [11] use a single collision avoidance/guidance strategy, Yang and Zhao [13] use a discrete search strategy, Vian and Moore and Twigg et al. [8,14] use cost proportional to distance from threats, and Raghunathan et al. [12] use an interior barrier penalty function technique to avoid no-fly zones. Because of the time criticality and multiple scenario analysis, an autonomous solution is desired over a manually iterative one. The research herein presents an optimal minimum time geometric trajectory solution based on a constrained maximum bank angle. The inclusion of an intermediate waypoint, or waypoints, distinguished this work from the earlier two-point boundary value research [15]. The geometric result developed herein is compared to a solution derived using dynamic optimization.

The dynamic optimization solution deviates from previous research [7,16,17] due to the inclusion of waypoints which are interior point constraints [6]. The difficulty that arises is that each waypoint is only an active constraint at the waypoint passage time which is unknown. This differs from the no-fly zones which are also constraints, however, they are valid for the duration of the flight. Although it may be tempting to simply optimize the flight between each waypoint, as will be shown, this will not yield the same solution as optimization over the entire trajectory. This comparison is quantified with a numerical example. The example used is a hypersonic vehicle at a constant altitude, that is, the vehicle is confined to a 2-D horizontal plane. This 2-D trajectory analysis could also be applied to other platforms such as nonhypersonic UAVs or ground vehicles.

This paper is broken up into multiple sections, each building upon the previous. Section II introduces the terminology used throughout this paper to describe various components of the problem and solution. It also includes the mission profile, the vehicle description, and the assumptions used to focus this research. Section III specifies the equations of motion and defines the three solution techniques: baseline, geometric, and dynamic optimization. Section IV expands upon the generic dynamic optimization technique defined in Sec. III. To demonstrate and compare these multiple methods, the results of a numerical example are presented in Sec. V. Finally, the significance of these results, and the research herein, is discussed in Sec. VI. The Appendix contains a supplemental proof of the constant speed geometric solution presented in Sec. III.

II. Mission and Vehicle

A. Terminology

The overall mission objective is to fly from an *initial* point to a *final* point, or *target*, in minimum time. The generic start point and finish point of a trajectory are called *endpoints*. For payload delivery or reconnaissance mission requirements, specified intermediate coordinates to fly over are *waypoints*. The vehicle must fly over each waypoint, also called waypoint *passage*; however, time, altitude, bank angle, and heading are not constrained. A *turnpoint* is defined as a discrete point where there is a change in the current constant control; therefore, the vehicle rolls into a turn or completes a turn at a turnpoint. There is no limit on the number of discrete changes in control, that is, turnpoints. The optimal solution presented herein dictates the number of turnpoints required. If waypoint passage occurs at some point within a constant control turn, the waypoint and turnpoints are not coincident. The entire trajectory can be broken up into sequential *legs* or *segments*, for example, between turnpoints. A *no-fly zone* is a region with a boundary that the vehicle must remain on or outside of. Because there can be multiple waypoints in a mission, each is numbered i, and the time of passage is denoted t_i. Similarly, there are j no-fly zones; however, the time of interest for each no-fly zone is t_j which is the time of no-fly zone entry, that is, boundary contact. The target is reached at the final time t_f and is called target *intercept*.

Table 1 Mission description

Descriptor	Latitude	Longitude	Radius
Initial	N 28° 34’	W 80° 38’	——
Waypoint 1	N 52° 11’	W 43° 46’	——
Waypoint 2	N 17° 01’	W 20° 33’	——
No-fly zone	N 22° 39’	E 11° 03’	840 n mile
Target	N 33° 46’	E 29° 34’	——

B. Mission

For the analysis, a specific mission is specified in Table 1 by its initial location, intermediate waypoints, no-fly zone(s), and final destination or target. The waypoints represent specified mission critical locations that must be flown over precisely, either for reconnaissance or for multiple payload deliveries. It is arguable that a vehicle may be limited to level flight for imaging or payload deployment; however, due to the long durations of the turns representative of the vehicle considered herein, a short level segment within the turn is approximated as a continuous turn. Therefore, in addition to no heading angle or altitude constraints, there is also no bank angle constraint at the waypoints. The no-fly zone coordinates are the center of the keep out circle with radius specified. The no-fly zones are infinite altitude; that is, no overflight at any altitude is permissible.

C. Mission and Model Assumptions

For the work presented, the following assumptions were made to scope the mission, equations of motion, and vehicle. Even though some assumptions deviate from an actual vehicle, for example, thrust without propellant (mass) loss, they are intended to keep the equations simpler so the new dynamic optimization derivations are easier to follow. This is the same rationale for allowing banking without increased drag; however, this assumption may be valid for other applications such as a nonskidding car. The assumptions are as follows:

1) The waypoints are specified in the desired sequence.

2) Inner-loop control is available. Only the outer loop or trajectory generation is addressed.

3) Waypoints are sufficiently spaced such that no two are within the turn radius of the vehicle.

4) The no-fly zones are specified as circular exclusion zones.

5) Mass, altitude, and gravity are constant.

6) The Earth is modeled as flat and nonrotating.

7) Acceleration (a) is either zero or constant.

8) Target intercept will occur in level flight, that is, the vehicle is not completing a waypoint turn and is not on a no-fly zone boundary.

D. Vehicle Description

The Hypersonic Cruise Vehicle (HCV) provides a platform with a large turn radius, enough thrust to oppose aerodynamic drag, and sufficient lift to provide a range of airspeeds to maintain level flight without stalling. The objective of the HCV is to deliver 12,000 lb of payload at a range of 9000 nautical miles (n mile) in 2 h [18,19]. An altitude of 100,000 ft is chosen because it was the approximate test altitude for the unmanned hypersonic Hyper-X (X-43A) test vehicle [20]. The range and time objectives equate to 2.315 km/s, which at flight level (FL1000) is Mach 7.66. The SR-71 is chosen as a representative high altitude, high Mach vehicle to determine other reasonable operational limitations. In the Operating Limitations section of the SR-71 Flight Manual [21], equivalent airspeed, expressed in knots equivalent airspeed (KEAS), is used to specify a minimum acceptable airspeed over a range of altitudes and Mach

numbers. This minimum is used to ensure sufficient airspeed to sustain level flight or engine performance. The minimum is $V_{\min} = 310$ KEAS, which equates to Mach 4.47 at FL1000. If a trajectory reaches the target at an airspeed less than $V_{\min}$ it is considered invalid because the constant altitude assumption would have been violated. For example, a flight starting at an initial airspeed of 2.315 km/s at FL1000, as described above, with a deceleration of 0.1 m/s^2 over 2 h has a final airspeed of 366 KEAS or Mach 5.28; thus the level flight assumption remains valid. A deceleration profile is chosen to demonstrate the effects of nonconstant velocity which leads to nonconstant turn radii. Also, deceleration will be a component of the eventual study of reentry profiles. The bank angle is limited to 20 deg due to wing loading, stability, and/or inlet airflow tolerances. A constant altitude is maintained by ensuring the vertical component of lift equals the vehicle weight, that is lift $= mg/\cos\sigma$. These derived parameters will be used as a representative HCV for demonstrating results.

III. Methodology

The goal of the research is to derive a technique of determining a trajectory that converges to an optimal solution, satisfies the waypoint and no-fly zone constraints, and requires minimal computational time. The trajectory is constrained by the equations of motion and available control authority. Altitude is constant so flight is confined to the horizontal (2-D) plane; this aspect is contained in the equations of motion because there is no altitude state. The bank angle control may be limited by structural loads, aerodynamic stability, or heating. This limitation on bank angle translates to a minimum turn radius to transition from one waypoint or no-fly zone to the next. The initial analysis assumes a constant speed which results in constant minimum turn radii. Later analysis allows for variable speed, thus varying turn radii.

A. Nondimensional Equations of Motion

For the analysis, scaling factors are used to create nondimensional variables from dimensional velocities, accelerations, distances, and time. The following scaling factors are more applicable to a spherical Earth model [22]; however, their use remains valid for this flat Earth model and the intent is to simplify the transition to a higher fidelity model for future research. The value of initial gravity (g_0) at the initial radius (r_0) from the center of the Earth is used as a scaling factor. For constant altitude, the generic gravity term g will equal g_0. The initial radius is the initial altitude above the Earth's surface plus the radius of the Earth. The initial gravity is corrected for altitude above the Earth's surface as $g_0 = g_{\text{surface}}(r_{\text{surface}}/r_0)^2$. Acceleration is normalized by g_0, velocity by $\sqrt{g_0 r_0}$, distances by r_0, and time by $\sqrt{r_0/g_0}$. Also, the normalized control is $u = \tan\sigma/\tan\sigma_{\max}$, where $\sigma_{\max}$ is the maximum bank angle. The nondimensional 2-D equations of motion are

$$\dot{x} = V\cos\theta \tag{1a}$$

$$\dot{y} = V\sin\theta \tag{1b}$$

$$\dot{\theta} = \frac{\tan\sigma_{\max}}{V}u \tag{1c}$$

$$\dot{V} = a \tag{1d}$$

B. Baseline

A baseline for comparison to the optimal solution is a simple steer-and-point approach to navigation. This equates to optimizing each segment [2,3] using a bang–level–bang control to satisfy the waypoints. This segment-by-segment technique is likely to unnecessarily fly an extended trajectory with overshoots following each waypoint passage, thus not optimized over the entire trajectory. The amount of time to be gained by optimizing over this baseline is proportional to the amount of time the vehicle is in turns compared to the total range. For a subsonic aircraft, with relatively small turn radii, the ratio of time within a turn is low and this optimization may produce a negligible time savings. However, the HCV has huge turn radii in comparison to its designed range and thus the time savings may be significant. The minimum time solution may also be beneficial to a fighter aircraft in confined terrain or a reconnaissance UAV with a small maximum bank angle.

C. Geometric, Constant Speed

First, a geometric solution is developed when navigating between two points containing an intermediate waypoint which is not collinear with the endpoints. For a vehicle flying a constant speed and bank angle past a waypoint, the 2-D horizontal trajectory follows a fixed turn radius circle, as depicted in Fig. 1. One possibility is for the waypoint passage to occur at the beginning of the turn, as shown in Fig. 1a. This would be the case for a pilot initiating a heading from P_1 directly toward the waypoint W_p, then at waypoint passage roll into a maximum bank turn in the direction of endpoint P_2, and finally completing the turn and rolling out at a heading aligned with P_2. This is the baseline case because it is a simple point–turn–point navigation

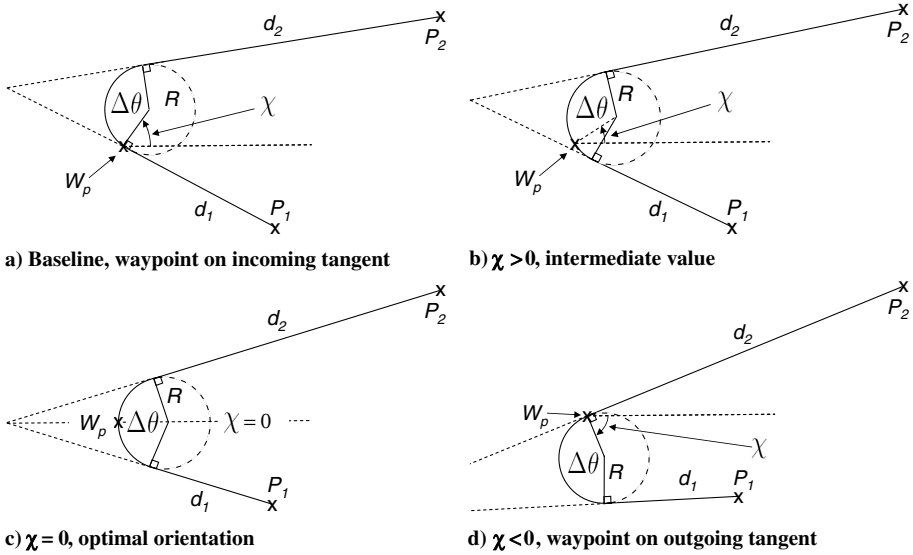

Fig. 1 Turn radius orientation rotated about the intermediate waypoint (W_p) by angle χ. Radius (R) is constant. Endpoints (P_1 and P_2), and intermediate waypoint (W_p) are fixed.

case. On the other extreme is the case where waypoint passage occurs at the end of the turn as in Fig. 1d. Of course, there are also cases where waypoint passage may occur somewhere along the turn as in Figs. 1b and 1c. The different points along the turn for waypoint passage are dictated by the orientation of the turn circle with respect to the waypoint W_p. To determine the optimal orientation of the turn circle, the case for two fixed endpoints and a fixed intermediate waypoint is analyzed, as shown in Fig. 1. For this analysis a constant speed is assumed; therefore, minimizing the flight path will minimize the flight time. The cost is the flight path length given by

$$J = d_1(\chi) + R\Delta\theta(\chi) + d_2(\chi) \tag{2}$$

where R is the specified turn radius and the values for d_1, d_2, and $\Delta\theta$ are all a function of angle χ. The turn radius is always rotated about the waypoint, thus ensuring passage. Also, the initial orientation ($\chi = 0$) is such that the intersection of the tangent lines from P_1 and P_2 is collinear with the waypoint and the center of the turn circle as shown in Fig. 1c. The angle χ is anchored at the waypoint and is measured counterclockwise to the center of the turn circle as shown in Fig. 1. A minimum of the cost J with respect to χ may exist when

$$\partial J/\partial\chi = 0 \tag{3}$$

Using purely geometric relations, the solution to Eq. (3) can be shown to exist at $\chi = 0$, for any values of the initial setup for P_1, P_2, W_p, and R. The significance of this result is that the minimum time trajectory can be analytically computed for any given initial, final, intermediate waypoint, and turn radius. Furthermore, at a constant velocity, the equations of motion do not need to be integrated, so long as a relationship between maximum bank angle and minimum turn radius exist. For an air vehicle to produce enough lift in a banked turn to maintain level flight, the centripetal acceleration a_c is lift $\sin\sigma/m$ where lift must be $mg/\cos\sigma$. Thus, for a nonskidding turn:

$$a_c = g\tan\sigma = \frac{V^2}{R} \tag{4}$$

thus

$$R = \frac{V^2}{g\tan\sigma} = \text{minimum turn radius} \tag{5}$$

In this geometric approach, the no-fly zones can be treated just like a minimum turn radius. If the no-fly zone radius is greater than the minimum turn radius, a tangent to the no-fly zone is flown. If the no-fly zone is smaller than the minimum turn radius, the no-fly zone is only touched in one place since flight along the boundary cannot be maintained.

As claimed, the optimal configuration shown in Fig. 1c can also be viewed geometrically as a circle inscribed within one of the vertices of a triangle. The center of an inscribed circle bisects the angle of each vertex [23]; therefore, the line from the vertex to the center of the circle is the angle bisector. This also implies, with respect to the center of the circle, that the angle from one tangent to the angle bisector is equal to the angle from the other tangent to the angle bisector. Thus, because the optimal waypoint in Fig. 1c lies on the angle bisector, the waypoint occurs halfway along the arc from the incoming tangent to the outgoing tangent. The optimality of this halfway point is proven in the Appendix.

In an application with multiple waypoints and no-fly zones, a simple iterative technique can be used to compute the optimal geometry. Initially select a value for χ, then compute the point of intersection of the two tangent lines. This provides a measure as to whether the intersection point was collinear with the waypoint and center of the radius. This is an iterative process because a tangent is made from the previous and following turn radii or no-fly zone. Because the intermediate waypoint turn radius orientation will change the points of tangency, the process continues until no more changes are required. Because no integration is required for the constant speed case, each iteration is fast, and convergence requires only a few iterations.

D. Geometric, Nonconstant Speed

For the case where speed is not constant, a modification to the above approach is required. For the equations of motion in Eq. (1), the minimum turn radius given in Eq. (5) will change with a change in velocity. Iterations are performed assuming a fixed turn radius based on the velocity achieved while starting the waypoint or no-fly zone turn. These new orientations are then simulated to determine the new entry velocities for each turn. The iteration was complete when a negligible change occurred in entry velocities. With deceleration, the vehicle is no longer confined to follow a fixed radius; thus this geometric solution is now a suboptimal solution because maximum bank angle is not always applied. To evaluate this against the true optimal solution a dynamic optimization technique is employed. As will be shown, the easily obtained geometric solution serves as an excellent initial guess when obtaining the optimal solution via dynamic optimization.

E. Dynamic Optimization

The dynamic optimization problem can be stated as minimizing a cost function subject to dynamic equation constraints, control inequality constraints, interior state equality constraints, interior state inequality constraints, and specified initial and final states [24]. The following sections systematically develop the framework for the 2-D optimization problem as outlined in Sec. II.B. Building upon this framework, the specific dynamic optimization solution for this problem is given in Sec. IV. A numerical example then follows in Sec. V.

F. Cost and Constraints

In general, the cost (J) is expressed as

$$J = \phi + \int_0^{t_f} L\,\mathrm{d}t \tag{6}$$

Relating this to the minimum time problem considered herein the free final time (t_f) is the cost, and the final position is a constraint ψ, such that,

$$\phi(\mathbf{x}(t_f), t_f) = t_f \tag{7}$$

$$L = 0$$

$$\psi(\mathbf{x}(t_f), t_f) = \begin{bmatrix} x(t_f) - x_f \\ y(t_f) - y_f \end{bmatrix} \tag{8}$$

The requirement to fly over each waypoint i establishes a set of state equality constraints. The time of waypoint passage (t_i) is unconstrained and must be determined as part of the optimal solution. The constraint to fly over the waypoint at time t_i implies the vehicle coordinates, $[x(t_i), y(t_i)]$, are equal to the specified waypoint coordinates, $[x_i, y_i]$. This is compactly written as

$$N(\mathbf{x}(t_i), t_i) = \begin{bmatrix} x(t_i) - x_i \\ y(t_i) - y_i \end{bmatrix} = 0 \qquad i = 1, 2, \ldots \tag{9}$$

Next, the requirement to stay outside each no-fly zone j establishes a state inequality constraint. This constraint is in effect for all times, t. Each no-fly zone j is defined as a circular region with center $[x_{cj}, y_{cj}]$ and time invariant radius R_j. This no-fly zone inequality constraint is expressed as

$$\begin{gathered} \Delta x = x(t) - x_{cj}, \qquad \Delta y = y(t) - y_{cj} \\ S(\mathbf{x}(t), t) = \tfrac{1}{2}\left(R_j^2 - \Delta x^2 - \Delta y^2\right) \le 0 \qquad j = 1, 2, \ldots \end{gathered} \tag{10}$$

Additionally, there is an inequality constraint on the control (u) to be within plus/minus the maximum normalized bank angle ($|u| \le 1$), as defined previously in Sec. III.A:

$$C(u(t), t)\begin{bmatrix} u - 1 \\ -u - 1 \end{bmatrix} \le 0 \tag{11}$$

Last, the no-fly zone inequality constraint imposes additional interior point constraints, namely, tangency constraints [24]. This implies a no-fly zone must be approached such that the no-fly zone is not violated upon reaching the boundary. For this example, the heading cannot be changed instantaneously; therefore, the no-fly zone must be approached on a tangent to avoid entering the no-fly zone. Thus, at boundary contact, from Eq. (10) $S = 0$, and the derivative or rate of change with respect to the no-fly zone must also be zero, $S^{(1)} = 0$. For the function in Eq. (10) the control appears in the second derivative of S, $S^{(2)}$, and dictates the control required to remain on the boundary, that is, to continue to satisfy all tangency constraints. The order of the derivative where the control generically appears is defined as q; thus, here $q = 2$. Each of the derivatives less than q, S to $S^{(q-1)}$, become the equality constraints. These take the same form as the waypoint constraints N but M will be used for distinction:

$$M(\mathbf{x}(t_j), t_j) = \begin{bmatrix} S(\mathbf{x}(t_j), t_j) \\ S^{(1)}(\mathbf{x}(t_j), t_j) \\ \vdots \\ S^{(q-1)}(\mathbf{x}(t_j), t_j) \end{bmatrix} = 0 \qquad j = 1, 2, \ldots \tag{12}$$

G. Hamiltonian

Once all the constraints are defined, the Hamiltonian is formed using multipliers to adjoin the dynamic equations and constraints. The constraints M and N represent the boundary or end condition for an intermediate segment, similar to the final constraint ψ; therefore, as with ψ, they do not appear in the Hamiltonian. These boundary conditions will be shown to define the final value of the costates (λ) at each segment. From the final value, the costates can be integrated backward in time to create a time history back to the initial time, t_0. The state and costate time history can be used to solve for the optimal solution. The multiplier μ_S will also need to be determined to propagate the costates (λ) backward in time. The vector μ_C is generically part of the Hamiltonian; however, it is shown later that for this problem it is not required for costate propagation. Using the state equations in Eq. (1), the Hamiltonian and state dynamics are given by

$$H = \lambda^T \dot{\mathbf{x}} + \mu_C^T C + \mu_S S^{(2)} \tag{13}$$

$$f = \dot{\mathbf{x}} = \begin{bmatrix} \dot{x} & \dot{y} & \dot{\theta} & \dot{V} \end{bmatrix}^T \tag{14}$$

The multipliers for the constraints are defined as follows. There are two components to the μ_C vector corresponding to the two constraints in Eq. (11). The first is nonzero when $u = 1$, but then $u - 1$ produces a zero product. When u is off the constraint, $u < 1$, μ_{C1} must be zero. The second multiplier μ_{C2} operates in the same fashion. The scalar μ_S works the same way for the value of $S^{(2)}$, where $S^{(2)} = 0$ corresponds to being on the no-fly zone constraint and $\mu_S = 0$ is off the constraint. Thus, the value of the Hamiltonian is not affected by these adjoined components; however, requisite partial derivatives are affected so these terms are not eliminated.

H. Control

The optimal control, used to generate the optimal trajectory, is determined by minimizing the Hamiltonian. Thus, the optimality condition is the derivative of the Hamiltonian with respect to u:

$$H_u = 0 \tag{15}$$

If the control does not explicitly appear in H_u, the Hamiltonian must be examined to determine the control required to minimize H. This is examined in Sec. IV.A.

I. Costates

The time history of the costates is required to either compute or verify the optimal control time history. The derivatives of the costates are used to integrate backward in time from the final costate values. The derivatives of the costates are defined based on the Hamiltonian in Eq. (13). The subscript $\mathbf{x}$ represents the derivative with respect to the state vector $\mathbf{x}$. The μ_C term does not appear because the constraint C is not a function of $\mathbf{x}$, $C_{\mathbf{x}} = 0$,

$$\dot{\lambda}^T = -H_{\mathbf{x}} = -\lambda^T f_{\mathbf{x}} - \mu_S S^{(2)}_{\mathbf{x}} \tag{16}$$

J. Final Costates and Transversality Condition

The final costates are used to anchor the backward in time propagation of the costates to create a time history of the costates. The final costates and transversality condition are functions of the final cost and final constraint in Eqs. (7) and (8). The final cost and constraint are adjoined with multipliers in vector ν:

$$\Phi = \phi + \nu^T \psi \tag{17}$$

The final costates are set equal to the partial derivative of Φ with respect to $\mathbf{x}$ [24]:

$$\lambda^T(t_f) = \Phi_{\mathbf{x}}(\mathbf{x}(t_f), t_f) = \phi_{\mathbf{x}}(\mathbf{x}(t_f), t_f) + \nu^T \psi_{\mathbf{x}}(\mathbf{x}(t_f), t_f) \tag{18}$$

and the transversality condition is the time derivative of Φ, defined as

$$\dot{\Phi}(\mathbf{x}(t_f), t_f) = \phi t_f + \Phi_{\mathbf{x}}(\mathbf{x}(t_f), t_f)\dot{\mathbf{x}}(\mathbf{x}(t_f)) = 0 \tag{19}$$

K. Jump Conditions

And last, intermediate boundary conditions for each waypoint and no-fly zone must be met. These interior constraints represent the terminal constraints for the previous segment, which occur at times t_i^- or t_j^-. Similar to the terminal constraints, at time t_f in Eq. (18), multipliers are introduced [24]. These multipliers present discontinuities or jumps in the costates to satisfy the interior state equalities, N and M. These jumps occur at waypoint passage times (t_i) and times of entry onto the no-fly zone boundaries (t_j) because these are the locations of the interior state constraints. At these same times there is also a jump in the Hamiltonian, but only if N and/or M are functions of time. The costates and Hamiltonian are continuous, that is, there are no jumps, at all other turnpoints; specifically, these are a completion of the initial heading correction, starting and completing a turn containing a waypoint, and exiting a no-fly zone. Thus, the jump conditions are defined as follows for each waypoint:

$$\lambda^T(t_i^-) = \lambda^T\left(t_i^+\right) + \pi_n^T \frac{\partial N}{\partial \mathbf{x}(t_i)} \tag{20}$$

$$H\left(t_i^-\right) = H\left(t_i^+\right) - \pi_n^T \frac{\partial N}{\partial t_i} \tag{21}$$

And for each no-fly zone:

$$\lambda^T\left(t_j^-\right) = \lambda^T\left(t_j^+\right) + \pi_m^T \frac{\partial M}{\partial \mathbf{x}(t_j)} \tag{22}$$

$$H\left(t_j^-\right) = H\left(t_j^+\right) - \pi_m^T \frac{\partial M}{\partial t_j} \tag{23}$$

The values in π_n and π_m may be different for each jump; however, the form of the equations remains the same. For the problem considered here, π_n has two elements for each waypoint and π_m has two elements for each no-fly zone; thus there are six constants to determine for the optimal solution.

IV. Solutions

The previous section provided the general framework for the dynamic optimization solution for the problem presented herein. To process a numerical example, additional solution steps are required and are contained in this section. The vectors ν, μ_C, μ_S, π_n, and π_m

are required to determine the optimal control and to propagate the costates using Eq. (16). Note that, for this problem μ_C does not appear in the costate propagation in Eq. (16). In this section the functional dependence $(\mathbf{x}(t), t)$ notation is removed for readability.

A. Control

The first task is to determine an optimal control u. The Hamiltonian in Eq. (13) can be multiplied out to show that there is only one term that is a function of u when not on a no-fly zone, that is, when $\mu_S = 0$,

$$H = \lambda_x V\cos\theta + \lambda_y V\sin\theta + \lambda_\theta \frac{\tan\sigma_{\max}}{V}u + \lambda_V a \tag{24}$$

The Pontryagin minimum principle yields that u must minimize H [25]. Furthermore, because the velocity V and the normalizing parameter $\tan\sigma_{\max}$ are always positive, u must be the maximum absolute value and opposite sign of λ_θ to minimize H. This defines λ_θ as the switching function for u in a bang–level–bang controller [26]. The optimal control specified below is only when the state is not on the no-fly zone constraint.

$$u^*(t) = \begin{cases} =1, & \lambda_\theta < 0 \\ =0, & \lambda_\theta = 0 \\ =-1, & \lambda_\theta > 0 \end{cases} \tag{25}$$

(This u^* is only applicable when off the no-fly zone constraints.)

To determine the control while on a no-fly zone constraint, first assume that the no-fly zone is larger than the minimum turn radius. This is not a limitation, it just implies that if the no-fly zone is smaller than the minimum turn radius than the optimal control would still be Eq. (25). The tangent entry requirement is specified as constraint M in Eq. (12), that is, $S = 0$ and $S^{(1)} = 0$. To remain on the no-fly zone constraint, the $S^{(2)} = 0$ condition must remain satisfied. For convenience Eq. (10) is repeated here as Eq. (26). Starting with Eq. (26), the chain rule and state derivatives in Eq. (1) are used to compute the time derivatives of S. Setting Eq. (28) equal to zero, the optimal control, u^*, along a no-fly zone boundary is computed in Eq. (29):

$$S = \tfrac{1}{2}\left(R_j^2 - \Delta x^2 - \Delta y^2\right) \tag{26}$$

$$S^{(1)} = -\Delta x V\cos\theta - \Delta y V\sin\theta \tag{27}$$

$$S^{(2)} = -V^2 + u(\Delta x\sin\theta - \Delta y\cos\theta)\tan\sigma_{\max} + (-\Delta x\cos\theta - \Delta y\sin\theta)a = 0 \tag{28}$$

$$u^*(t) = \frac{V^2}{(\Delta x\sin\theta - \Delta y\cos\theta)\tan\sigma_{\max}} \tag{29}$$

(This u^* is only applicable while on a no-fly zone constraint.) The term in front of a in Eq. (28) is zero, because it is a multiple of Eq. (27), which is identically zero when tangent to the no-fly zone boundary. It is not eliminated from Eq. (28) because the partial derivative of $S^{(2)}$ with respect to the state vector is still required to propagate the costates.

B. Costate Propagation

The derivative of the costates must be determined in order to propagate the costates backward in time. The costate time history is used to compute the optimal control time history. Substituting the partial derivative of Eqs. (14) and (28) into the transpose of Eq. (16) produces

$$\dot{\lambda} = [-\lambda^T f_{\mathbf{x}}]^T - \mu_S\left[S_{\mathbf{x}}^{(2)}\right]^T$$

$$\begin{bmatrix}\dot{\lambda}_x\\ \dot{\lambda}_y\\ \dot{\lambda}_\theta\\ \dot{\lambda}_V\end{bmatrix} = \begin{bmatrix}0\\ 0\\ \lambda_x V\sin\theta - \lambda_y V\cos\theta\\ -\lambda_x\cos\theta - \lambda_y\sin\theta + \lambda_\theta\frac{\tan\sigma_{\max}}{V^2}u\end{bmatrix} - \mu_S\begin{bmatrix}u\sin\theta\tan\sigma_{\max} - a\cos\theta\\ -u\cos\theta\tan\sigma_{\max} - a\sin\theta\\ (\Delta x\sin\theta - \Delta y\cos\theta)a\\ -2V\end{bmatrix} \tag{30}$$

If not on a no-fly zone boundary, then $\mu_S = 0$ and only the first term in Eq. (30) needs to be propagated. However, if on a no-fly zone constraint, then $\mu_S \neq 0$ and its value must be computed. Solving for $H_u = 0$ as the partial derivative of H in Eq. (13) with respect to u yields

$$\mu_s = \frac{-\lambda_\theta}{V(\Delta x\sin\theta - \Delta y\cos\theta)} \tag{31}$$

C. Final Costates

The costates are initialized at the final time, t_f, to begin the backward-in-time integration. The vector ν contains two elements, ν_x and ν_y, because there are two elements of the final constraint ψ. From the final costate equation (18), with $\phi_{\mathbf{x}} = 0$ and ψ only a function of x and y, the final costates can simply be defined as

$$\begin{bmatrix}\lambda_x(t_f) & \lambda_y(t_f) & \lambda_\theta(t_f) & \lambda_V(t_f)\end{bmatrix} = \begin{bmatrix}\nu_x & \nu_y & 0 & 0\end{bmatrix} \tag{32}$$

Stated in Sec. II.C, it is assumed that at target intercept the vehicle is not in a turn, then $u(t_f) = 0, \lambda_\theta(t_f) = 0$, and $\dot{\lambda}_\theta(t_f) = 0$. Substitution of ν_x and ν_y into the transversality condition (19), and $\dot{\lambda}_\theta(t_f) = 0$ into Eq. (30), leads to

$$\lambda_x(t_f) = \nu_x = \frac{-\cos\theta_f}{V_f} \tag{33a}$$

$$\lambda_y(t_f) = \nu_y = \frac{-\sin\theta_f}{V_f} \tag{33b}$$

Also, because the Hamiltonian is not explicitly a function of time it must be a constant. Therefore, solving the transversality condition in Eq. (19) and substituting $\lambda(t_f)$ from Eq. (18) into H at t_f in Eq. (13), the constant for H is completely determined as

$$H(t_f) = H(t) = -1 \tag{34}$$

D. Jump Conditions

Next, the boundary conditions at the end of each segment must be satisfied. To satisfy the intermediate boundary conditions N and M, there is a jump in the costates at times t_i and t_j. The jumps occur at each waypoint passage and enter onto the tangent of each no-fly zone constraint. The control is continuous if waypoint passage occurs along the turn, that is, $u(t_i^-) = u(t_i^+)$. Because the assumption is that the waypoints are sufficiently spaced, the control is zero just before starting the turn, $u(t_{si}^-) = 0$, and nonzero immediately upon commencing the turn, $u(t_{si}^+) \neq 0$. Similarly for the no-fly zone, the control is zero immediately before entering the no-fly zone boundary, $u(t_j^-) = 0$, and nonzero immediately after contact, $u(t_j^+) \neq 0$. From the optimal control, $u^*(t)$, the definition in Eq. (25), any time the control is zero the switching costate (λ_θ) is zero. Additionally, the states are continuous, and for this problem the Hamiltonian is continuous, as derived from Eqs. (21) and (23). Thus, the costate jump at each waypoint is given in terms of the unknown constants, π_{nx} and π_{ny}:

$$\lambda\left(t_i^-\right)^T = \lambda\left(t_i^+\right)^T + \begin{bmatrix} \pi_{nx} & \pi_{ny} & 0 & 0 \end{bmatrix} \tag{35}$$

The costate propagation in Eq. (30) shows $\dot{\lambda}_x = \dot{\lambda}_y = 0$; therefore, the costates λ_x and λ_y do not change from the start of the waypoint turn to immediately before the waypoint passage (referencing forward in time):

$$\lambda_x(t_{si}) = \lambda_x\left(t_i^-\right) = \lambda_x\left(t_i^+\right) + \pi_{nx} \tag{36a}$$

$$\lambda_y(t_{si}) = \lambda_y\left(t_i^-\right) = \lambda_y\left(t_i^+\right) + \pi_{ny} \tag{36b}$$

Using the Hamiltonian and Eq. (36) there exists a relationship between the heading at the start of the turn, θ_{si}, and the heading at the jump, θ_i. From Eq. (21) it is determined that $H(t_i^-) = H(t_i^+)$. Using Eqs. (30) and (36) with $\dot{\lambda}_\theta(t_{si}) = 0$ and $\lambda(t_i^+)$ obtained by integrating backward in time from t_f, the constants are

$$\pi_{nx} = \frac{-\sin\theta_i\left(\lambda_x\left(t_i^+\right)\sin\theta_{si} - \lambda_y\left(t_i^+\right)\cos\theta_{si}\right)}{\cos(\theta_i - \theta_{si})} + \frac{\cos\theta_{si}\lambda_\theta\left(t_i^+\right)\tan\sigma_{\max}\left(u\left(t_i^+\right) - u\left(t_i^-\right)\right)}{V_{si}^2} \tag{37a}$$

$$\pi_{ny} = \frac{\cos\theta_i\left(\lambda_x\left(t_i^+\right)\sin\theta_{si} - \lambda_y\left(t_i^+\right)\cos\theta_{si}\right)}{\cos(\theta_i - \theta_{si})} + \frac{\sin\theta_{si}\lambda_\theta\left(t_i^+\right)\tan\sigma_{\max}\left(u\left(t_i^+\right) - u\left(t_i^-\right)\right)}{V_{si}^2} \tag{37b}$$

When waypoint passage occurs along the turn, $u(t_i^-) = u(t_i^+)$, and only the first terms in Eq. (37) are nonzero. Note that the baseline trajectory defined in Sec. III.B is a special case, where the passage of each waypoint occurs at the start of the turn, that is, $t_{si} = t_i$ and $\theta_{si} = \theta_i$, but the turn just commenced so $u(t_i^-) \neq u(t_i^+)$; thus, the terms at the end of Eq. (37) are nonzero. Recall the baseline is a simple nonoptimized steer and point control, so dynamic optimization is not required. Therefore, this special case is only included for completeness to allow the reader to compute the Hamiltonian for the baseline to see how it compares to the optimal Hamiltonian.

For the no-fly zone constraint, the components of M in Eq. (12) must be satisfied:

$$M = \begin{bmatrix} S \\ S^{(1)} \end{bmatrix} = \begin{bmatrix} \frac{1}{2}\left(R_j^2 - \Delta x^2 - \Delta y^2\right) \\ -\Delta x V\cos\theta - \Delta y V\sin\theta \end{bmatrix} = \begin{bmatrix} 0 \\ 0 \end{bmatrix} \tag{38}$$

The control is zero approaching the no-fly zone, which implies λ_θ has been zero, and thus the entry has the property that $\dot{\lambda}_\theta(t_j^-) = 0$. Also, like the waypoint jump, the Hamiltonian is constant $H(t_j^-) = H(t_j^+)$. Taking the partial derivatives of M in Eq. (22) and solving for the constants using $\lambda_\theta(t_j^-) = 0$, $\dot{\lambda}_\theta(t_j^-) = 0$, and $H(t_j^-) = H(t_j^+)$ leads to the following:

$$\Delta x_j = x(t_j) - x_{cj}, \qquad \Delta y_j = y(t_j) - y_{cj} \tag{39}$$

$$\begin{bmatrix} \lambda_x(t_j^-) \\ \lambda_y(t_j^-) \\ \lambda_\theta(t_j^-) \\ \lambda_V(t_j^-) \end{bmatrix} = \begin{bmatrix} \lambda_x\left(t_j^+\right) - \pi_{m0}\Delta x_j - \pi_{m1}V_j\cos\theta_j \\ \lambda_y\left(t_j^-\right) - \pi_{m0}\Delta y_j - \pi_{m1}V_j\sin\theta_j \\ \lambda_\theta\left(t_j^-\right) + \pi_{m1}(\Delta x_j\sin\theta_j - \Delta y_j\cos\theta_j)V_j \\ \lambda_V\left(t_j^+\right) \end{bmatrix} \tag{40}$$

$$\pi_{m0} = \frac{\lambda_x\left(t_j^+\right)\sin\theta_j - \lambda_y\left(t_j^+\right)\cos\theta_j}{\Delta x_j\sin\theta_j - \Delta y_j\cos\theta_j} \tag{41}$$

$$\pi_{m1} = \frac{\lambda_\theta\left(t_j^+\right)u\left(t_j^+\right)\tan\sigma_{\max}}{V_j^3} = \frac{-\lambda_\theta\left(t_j^+\right)}{V_j(\Delta x_j\sin\theta_j - \Delta y_j\cos\theta_j)} \tag{42}$$

Because the states at time t_j are continuous, the plus and minus superscripts are unnecessary. The control $u(t_j^+)$ in Eq. (42) is replaced with the u required to maintain $S^{(2)} = 0$ from Eq. (29). Within the derivation of Eq. (42), additional terms appear that are multiples of $S^{(1)}$; however, because $S^{(1)} = 0$ these terms are not shown for simplification.

Having now defined all the criteria for the optimal trajectory, the next step is to connect all the solution pieces. The geometric solution provides an initial guess of the 10 solution times; the waypoint passage times (2), the no-fly zone entry time (1), the final time (1), the end of the initial turn toward the first waypoint (1), the start and end time of each waypoint turn (4), and the no-fly zone exit time (1). These times, and the associated optimal control, are used to propagate the states forward. From the forward integration, the accuracy of hitting the final target, Eq. (8), passing through each waypoint, Eq. (9), and satisfying the tangency conditions, Eq. (12), are all used as the measure of solution success. At this point, for the mission as defined in Table 1, the solution has eight separate criteria. The forward states are interpolated during the backward integration for the costates. During the backward integration, the appropriate derivatives and jumps are computed. The accuracy of achieving each $\lambda_\theta(t_{si}^-) = 0$ is additional solution criteria: two for this mission because there are two waypoints. This increases the total number of solution criteria to 10. Thus, a search vector of 10 times is used to satisfy 10 success criteria, which should each be zero. A root solver can be used to manipulate a search vector to drive a solution vector to zeros. For this research, the solution or search times are input into the MATLAB® root solver, fsolve, to drive the solution criteria toward zero. A related indication of success (optimality) is to observe the value of the Hamiltonian. During this derivation, $H(t)$ is assumed continuous, but only the optimal solution will yield $H(t) = -1$ from Eq. (34) for all t. The results from this process are presented in the next section.

V. Results

To illustrate the time savings possible using optimal control, several HCV trajectories based on the mission described in Table 1 are presented in Fig. 2. For this problem the initial heading is fixed and the final heading is not constrained; therefore, the optimization is the orientation angle for the turn radii of the first and second intermediate waypoints and the point entering the no-fly zone boundary. The baseline, geometric, and dynamic optimization numerical results are presented in Table 2. For constant speed, the geometric and dynamic optimization results are identical, as derived in the Appendix. With deceleration, the geometric and dynamic optimization results are nearly the same, and are thus indistinguishable in Fig. 2.

The variable u becomes a bang–level–bang control based on the value of the costate λ_θ. In Fig. 3a the value of u switches with the sign of λ_θ. The exception to the bang–level–bang control is while the trajectory is on the no-fly zone boundary. The value of u is less than the maximum to avoid violating the constraint; however, optimality is maintained since $H_u = 0$ is maintained by Eq. (31).

In Fig. 3b the effect of a nonoptimal solution is demonstrated by observing the value of the Hamiltonian. Here, the optimal solution correctly maintains a Hamiltonian value of -1; however, with deceleration the geometric solution is seen to be nonoptimal. Nonoptimality is expected with the geometric solution because it forces constant turn radii. However, this no longer represents a maximum bank angle turn while decelerating. The baseline

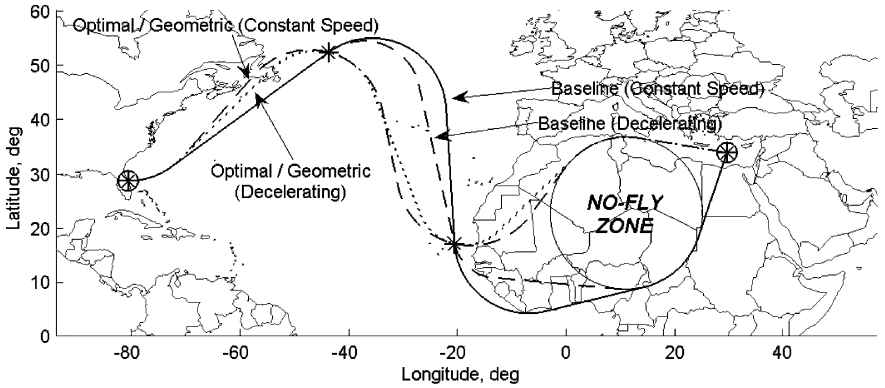

Fig. 2 Baseline, geometric, and optimal trajectories, both constant speed and decelerating.

Hamiltonian, not plotted, is even further from optimal reaching a Hamiltonian value of 1.04 (that is 2.04 from the optimal value of −1).

In Table 2 there are some notable trends beyond just minimizing flight time. For the constant speed baseline case, the vehicle does not meet the design specifications of 9000 n mile in 2 h. So, not only does the baseline take 14% longer, it fails the mission. A mission failure may be characterized by consuming all fuel before reaching the target. A similar time savings is seen with the decelerating case; however, the baseline is unsatisfactory because it has reached an airspeed too slow to sustain level flight ($V_{\min} \geq 310$ KEAS for level flight), thus this trajectory is invalid. Once again, the optimized trajectory has not only saved time, but enabled mission success. Table 3 is provided as a means of verifying duplication of the presented results.

VI. Conclusions

These results show that improvement can be made over the baseline trajectory. The amount of improvement will be proportional to the amount of time the vehicle is in a turn compared to the total flight time. The results also show that mission success may be dependent on finding an optimal solution versus settling for the baseline trajectory. For low deceleration rates, thus approximately circular turn radii, the geometric technique provides a near optimal solution at a fraction of the dynamic optimization computational time. Therefore, the geometric solution may prove valuable as an initial guess to another optimization routine. The dynamic optimization technique does provide an optimal solution, and it may be used as a valuable tool to determine how close the geometric solution (or any other solution) is to optimal. Additional studies may show that the computational savings using the geometric technique could significantly outweigh the small nonoptimality. Future work may include generalizing the geometric solution to other problems and/or increasing the number of degrees of freedom.

Appendix: Proof of Optimality

For the constant speed case, the optimal turn radius orientation is stated as the waypoint occurring halfway between the initiation and completion of the turn (see Fig. 1c in Sec. III.C). The geometric derivation of $\chi = 0$ is rather laborious; however, the following are two alternative derivations.

Dynamic optimization shows a bang–level–bang solution, meaning the control is either zero or at a maximum left or right bank angle. At constant velocity, a bang–level–bang control trajectory is seen in Fig. 4. The initial, waypoint, and final points are fixed: $[x_0, y_0]$, $[x_w, y_w]$, and $[x_f, y_f]$, respectively. The initial angle θ_0 and final angle θ_f are free. The fraction of time along the turn that waypoint passage occurs is also free and must be determined for the optimal solution. Let the waypoint passage occur at some fraction (k) between starting the turn ($k = 0$) and exiting the turn ($k = 1$); therefore, the heading angle at waypoint passage is $\theta_0 + k(\theta_f - \theta_0)$. For example, in Sec. III.C, Fig. 1a is $k = 0$, Fig. 1b is $k \approx 1/4$, Fig. 1c is $k = 1/2$, and Fig. 1c is $k = 1$. Let the time of flight from the initial point to the start of the turn be T_0 and the time of flight from the exit of the turn to the final point be T_f. During the level portions of flight the control is zero, and during a turn the control is ± 1 which is retained generically as u.

I. Proof Method 1: Equations of Motion

The following derivation integrates the equations of motion from the initial point to the waypoint depicted in Fig. 4, then to the final point. The nondimensional equations of motion are Eq. (1) with $\dot{V} = 0$. These equations can be integrated from the initial point to the waypoint:

$$x_w = x_0 + T_0 V \cos\theta_0 - \frac{V^2}{u \tan\sigma_{\max}} \sin\theta_0 + \frac{V^2}{u \tan\sigma_{\max}} \sin[\theta_0 + k(\theta_f - \theta_0)] \tag{A1a}$$

$$y_w = y_0 + T_0 V \sin\theta_0 + \frac{V^2}{u \tan\sigma_{\max}} \cos\theta_0 - \frac{V^2}{u \tan\sigma_{\max}} \cos[\theta_0 + k(\theta_f - \theta_0)] \tag{A1b}$$

The second set of equations specifies the path from the waypoint to the final:

Table 2 Numerical results for each trajectory 9000 n mile in 2 h at 100,000 ft

$V_{\min} = 310$ KEAS, initial conditions: $\theta_0 = 0$ deg, $M_0 = 7.66$
$V_0 = 2.315$ km/s, $r_0 = 6408.48$ km, $g_0 = 9.7169$ m/s^2

Technique	Decel, m/s^2	V_f KEAS	M_f	Distance, n mile	Time, hh:mm:ss
Baseline	0	531.69	7.66	10285	02:17:08
Geometric	0	531.69	7.66	9000	02:00:00
Optimal	0	531.69	7.66	9000	02:00:00
Baseline[a]	0.1	301.31	4.34	9822	02:47:11
Geometric	0.1	331.24	4.78	8853	02:25:28
Optimal	0.1	331.89	4.78	8831	02:24:59

[a]Invalid solution because minimum airspeed for level flight ($V_{\min}$) is not maintained.

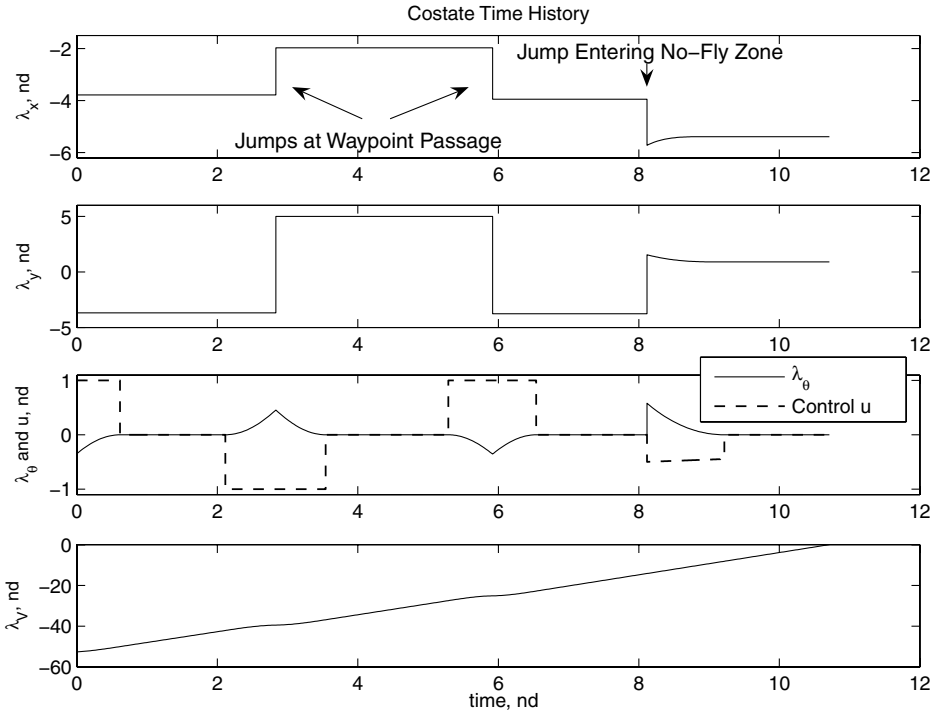

a) Costates and control *u* time history for dynamic optimal control of decelerating flight

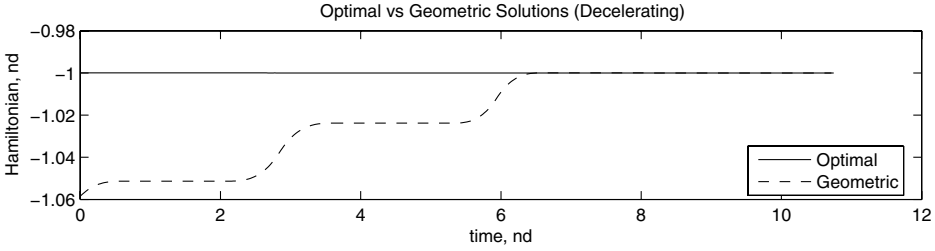

b) Optimal Hamiltonian $H(t) = -1$, and nonoptimal $H(t) \neq -1$

Fig. 3 Nondimensional (nd) costates, control, and Hamiltonian time histories.

$$x_f = x_w - \frac{V^2}{u \tan \sigma_{\max}} \sin[\theta_0 + k(\theta_f - \theta_0)] + \frac{V^2}{u \tan \sigma_{\max}} \sin \theta_f + T_f V \cos \theta_f \tag{A2a}$$

$$y_f = y_w + \frac{V^2}{u \tan \sigma_{\max}} \cos[\theta_0 + k(\theta_f - \theta_0)] - \frac{V^2}{u \tan \sigma_{\max}} \cos \theta_f + T_f V \sin \theta_f \tag{A2b}$$

The leg time T_0 is solved from Eq. (A1) and the leg time T_f is solved from Eq. (A2):

$$\begin{aligned} T_0 &= \frac{1}{V}\left\{(x_w - x_0)\cos\theta_0 + (y_w - y_0)\sin\theta_0 - \frac{V^2}{u \tan \sigma_{\max}} \sin[k(\theta_f - \theta_0)]\right\} \\ T_f &= \frac{1}{V}\left\{(x_f - x_w)\cos\theta_f + (y_f - y_w)\sin\theta_f - \frac{V^2}{u \tan \sigma_{\max}} \sin[(1-k)(\theta_f - \theta_0)]\right\} \end{aligned} \tag{A3}$$

The time in the turn is $V(\theta_f - \theta_0)/(u \tan \sigma_{\max})$, so the total cost ($J$) is the time from the initial point, through the waypoint in Fig. 4, to the final point:

Table 3 Nondimensional times for turns and target arrival

Technique	Initial End	Waypoint 1 Start	Waypoint 1 Pass	Waypoint 1 End	Waypoint 2 Start	Waypoint 2 Pass	Waypoint 2 End	No-fly zone Enter	No-fly zone Exit	Target Arrive
Baseline	0.507	2.616	2.616	4.339	5.819	5.819	7.228	8.328	9.157	10.132
Geometric	0.688	1.843	2.738	3.633	4.487	5.415	6.344	6.984	7.894	8.866
Optimal	0.688	1.843	2.738	3.633	4.487	5.415	6.344	6.984	7.894	8.866
Baseline	0.502	2.748	2.748	4.149	6.323	6.323	7.099	9.031	10.713	12.352
Geometric	0.641	2.084	2.842	3.624	5.276	5.940	6.623	8.129	9.250	10.747
Optimal	0.615	2.114	2.834	3.542	5.288	5.918	6.539	8.116	9.218	10.712

All trajectories $t_0 = 0$. First three entries are constant speed, last three are decelerating.

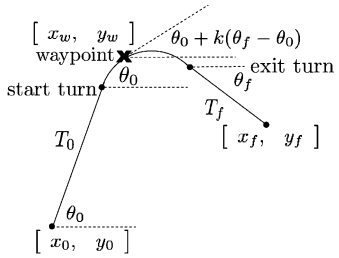

Fig. 4 A constant speed trajectory from an initial point at a heading θ_0, passing through and intermediate waypoint, and completing the turn at a heading θ_f to intercept a final point.

$$J = T_0 + V(\theta_f - \theta_0)/(u \tan \sigma_{\max}) + T_f \tag{A4}$$

To minimize the cost with respect to the waypoint passage fraction (k), the partial derivative of J with respect to k must be zero, that is, $\partial J/\partial k = 0$. Assume $\theta_f \neq \theta_0$ because that would imply a straight line or no turn. Performing the partial derivative:

$$\frac{\partial J}{\partial k} = -\frac{V}{u \tan \sigma_{\max}}(\theta_f - \theta_0)\cos[k(\theta_f - \theta_0)] + \frac{V}{u \tan \sigma_{\max}}(\theta_f - \theta_0)\cos[(1-k)(\theta_f - \theta_0)] = 0$$

While in the turn the control u, the speed V, the maximum bank angle $\theta_{\max}$, and the term $(\theta_f - \theta_0)$ are all nonzero, so division by these terms remains valid:

$$\cos[k(\theta_f - \theta_0)] = \cos[(1-k)(\theta_f - \theta_0)]$$
$$k(\theta_f - \theta_0) = (1-k)(\theta_f - \theta_0) \qquad k = 1/2$$

This shows that the optimal waypoint passage occurs halfway through the turn, which has the geometric properties shown in Fig. 1c.

II. Proof Method 2: Dynamic Optimization

Dynamic optimization uses dynamics, terminal, and intermediate state constraints to formulate the problem. With only one waypoint, and without considering a no-fly zone, this is a simplified version of the problem generically derived in Sec. IV. The cost to minimize is final time (t_f) and the heading to determine for the optimal solutions is θ_w, which occurs at the waypoint passage time (t_w). The nondimensional equations of motion are Eq. (1) with $\dot{V} = 0$. The terminal and waypoint constraint are ψ and N, respectively,

$$\psi = \begin{bmatrix} x(t_f) - x_f \\ y(t_f) - y_f \end{bmatrix} \qquad N = \begin{bmatrix} x(t_w) - x_w \\ y(t_w) - y_w \end{bmatrix} \tag{B1}$$

The Hamiltonian is

$$H = \lambda_x V \cos\theta + \lambda_y V \sin\theta + \lambda_\theta \frac{\tan \sigma_{\max}}{V} u$$

The following are Eqs. (30) and (33) without the velocity dynamics and with $\mu_S = 0$ (outside no-fly zones):

$$\dot{\lambda}_x = 0 \qquad \lambda_x(t_f) = -\cos\theta_f/V \qquad \dot{\lambda}_y = 0$$
$$\lambda_y(t_f) = -\sin\theta_f/V \qquad \dot{\lambda}_\theta = \lambda_x V \sin\theta - \lambda_y V \cos\theta$$
$$\lambda_\theta(t_f) = 0$$

Equation (37) is the solution for the jump in costates. Because there is only one waypoint, $\theta_i = \theta_w$ and $t_i^+ = t_w^+$. For waypoint passage between initial and final states, the control is constant over the jump, that is, $u(t_w^-) = u(t_w^+)$. Because λ_x and λ_y are constants (excluding the jumps), $\lambda_x(t_w^+) = \lambda_x(t_f)$ and $\lambda_y(t_w^+) = \lambda_y(t_f)$. At the start of the turn (t_{si}^-), the heading is $\theta_{si} = \theta_0$. The jump in costates λ_x and λ_y are

$$\pi_{nx} = \frac{-\sin\theta_w\left(\lambda_x\left(t_w^+\right)\sin\theta_{si} - \lambda_y\left(t_w^+\right)\cos\theta_{si}\right)}{\cos(\theta_w - \theta_{si})} = \frac{-\sin\theta_w(-\cos\theta_f \sin\theta_0 + \sin\theta_f \cos\theta_0)}{V\cos(\theta_w - \theta_0)} = -\sin\theta_w \frac{\sin(\theta_f - \theta_0)}{V\cos(\theta_w - \theta_0)} \tag{B2a}$$

$$\pi_{ny} = \frac{\cos\theta_w\left(\lambda_x\left(t_w^+\right)\sin\theta_{si} - \lambda_y\left(t_w^+\right)\cos\theta_{si}\right)}{\cos(\theta_w - \theta_{si})} = \frac{\cos\theta_w(-\cos\theta_f \sin\theta_0 + \sin\theta_f \cos\theta_0)}{V\cos(\theta_w - \theta_0)} = \cos\theta_w \frac{\sin(\theta_f - \theta_0)}{V\cos(\theta_w - \theta_0)} \tag{B2b}$$

Therefore the costates behind the jump at t_w^-, going backward in time, are

$$\lambda_x\left(t_w^-\right) = -\frac{\cos\theta_f}{V} - \sin\theta_w \frac{\sin(\theta_f - \theta_0)}{V\cos(\theta_w - \theta_0)}$$
$$\lambda_x\left(t_w^-\right) = -\frac{\sin\theta_f}{V} + \cos\theta_w \frac{\sin(\theta_f - \theta_0)}{V\cos(\theta_w - \theta_0)}$$

Substitute these values into the Hamiltonian at the start of the turn (t_{si}^-), where $u(t_{si}^-) = 0$, $\dot{x}(t_{si}^-) = V\cos\theta_0$, and $\dot{y}(t_{si}^-) = V\sin\theta_0$; then set the Hamiltonian equal to -1. The Hamiltonian and the states are continuous so the plus and minus superscript notation is unnecessary,

$$H(t_{si}) = \left(-\cos\theta_f - \sin\theta_w \frac{\sin(\theta_f - \theta_0)}{\cos(\theta_w - \theta_0)}\right)\cos\theta_0 + \left(-\sin\theta_f + \cos\theta_w \frac{\sin(\theta_f - \theta_0)}{\cos(\theta_w - \theta_0)}\right)\sin\theta_0 = -1$$
$$-(\cos\theta_f \cos\theta_0 + \sin\theta_f \sin\theta_0) - (\sin\theta_w \cos\theta_0 - \cos\theta_w \sin\theta_0)\frac{\sin(\theta_f - \theta_0)}{\cos(\theta_w - \theta_0)} = -1$$
$$\cos(\theta_f - \theta_0)\cos(\theta_w - \theta_0) + \sin(\theta_f - \theta_0)\sin(\theta_w - \theta_0) = \cos(\theta_w - \theta_0)$$
$$\cos(\theta_f - \theta_0 - \theta_w + \theta_0) = \cos(\theta_w - \theta_0)$$
$$\theta_f - \theta_w = \theta_w - \theta_0$$
$$\theta_w = \frac{\theta_f + \theta_0}{2} = \theta_0 + \frac{1}{2}(\theta_f - \theta_0) \tag{B3}$$

Because θ_w is of the form $\theta_0 + k(\theta_f - \theta_0)$, the optimal solution is again shown to be $k = 1/2$. This solution for θ_w can be plugged back into the jump equation, Eq. (B2), to solve for π_{nx} and π_{ny}. With a solution for the jumps, the value of the costates at t_w^- can be computed. For one waypoint this provides the value of the initial costates at t_0; $\lambda_x(t_0) = -\cos\theta_0/V$, $\lambda_y(t_0) = -\sin\theta_0/V$, and $\lambda_\theta(t_0) = 0$.

Acknowledgments

The research presented in this document is sponsored by the U.S. Air Force Research Laboratory's Space Vehicles Directorate, under the direction of Russell Partch and T. Alan Lovell.

References

[1] USAF, "Air Force Handbook—109th Congress," Department of the Air Force, Washington, D.C., 2005.

[2] Erzberger, H., and Lee, H. Q., "Optimum Horizontal Guidance Techniques for Aircraft," *Journal of Aircraft*, Vol. 8, No. 2, Feb. 1971, pp. 95–101.

[3] Shapira, I., and Ben-Asher, J. Z., "Near-Optimal Horizontal

Trajectories for Autonomous Air Vehicles," *Journal of Guidance, Control, and Dynamics*, Vol. 20, No. 4, July–Aug. 1997, pp. 735–741.

[4] Innocenti, M., Pollini, L., and Turra, D., "Guidance of Unmanned Air Vehicles Based on Fuzzy Sets and Fixed Waypoints," *Journal of Guidance, Control, and Dynamics*, Vol. 27, No. 4, 2004, pp. 715–720.

[5] Whang, I. H., and Whang, T. W., "Horizontal Waypoint Guidance Design Using Optimal Control," *IEEE Transactions on Aerospace and Electronic Systems*, Vol. 38, No. 3, July 2002, pp. 1116–1120. doi:10.1109/TAES.2002.1039430

[6] Moon, G., and Kim, Y., "Optimum Flight Path Design Passing Through Waypoints for Autonomous Flight Control System," AIAA 2003-5334, 11–13 Aug. 2003.

[7] Yang, H., and Zhao, Y. J., "Efficient Trajectory Synthesis Through Specified Waypoints," *AIAA 3rd "Unmanned Unlimited" Technical Conference*, AIAA, Reston, VA, 20–23 Sept. 2004.

[8] Vian, J. L., and Moore, J. R., "Trajectory Optimization with Risk Minimization for Military Aircraft," *Journal of Guidance, Control, and Dynamics*, Vol. 12, No. 3, May–June 1989, pp. 311–317.

[9] Bortoff, S. A., "Path Planning for UAVs," *Proceedings of the American Control Conference*, IEEE, Piscataway, NJ, June 2000.

[10] Judd, K. B., and McLain, T. W., "Spline Based Path Planning for Unmanned Air Vehicles," AIAA 2001-4238, 2001.

[11] Kumar, B. A., and Ghose, D., "Radar-Assisted Collision Avoidance-Guidance Strategy for Planar Flight," *IEEE Transactions on Aerospace and Electronic Systems*, Vol. 37, No. 1, Jan. 2001, pp. 77–89. doi:10.1109/7.913669

[12] Raghunathan, A. U., Gopal, V., Subramanian, D., Biegler, L. T., and Samad, T., "3D Conflict Resolution of Multiple Aircraft via Dynamic Optimization," *AIAA Guidance, Navigation, and Control Conference and Exhibit*, AIAA, Reston, VA, 11–14 Aug. 2003.

[13] Yang, H. I., and Zhao, Y. J., "Trajectory Planning for Autonomous Aerospace Vehicles amid Known Obstacles and Conflicts," *Journal of Guidance, Control, and Dynamics*, Vol. 27, No. 6, Nov.–Dec. 2004, pp. 997–1008.

[14] Twigg, S., Calise, A., and Johnson, E., "On-Line Trajectory Optimization Including Moving Threats and Targets," AIAA 2004-5139, 2004.

[15] Dubins, L. E., "On Curves of Minimal Length with a Constraint on Average Curvature, and with Prescribed Initial and Terminal Positions and Tangents," *American Journal of Mathematics*, Vol. 79, No. 3, July 1957, pp. 497–516. doi:10.2307/2372560

[16] Bryson, A. E., Jr., *Dynamic Optimization*, Addison Wesley Longman, Reading, MA, 1999.

[17] Bryson, A. E., Jr., *Applied Linear Optimal Control: Examples and Algorithms*, Cambridge Univ. Press, Cambridge, England, U.K., 2002.

[18] DARPA/USAF, "Northrop Grumman Takes Aim at Hypersonic Weapon Delivery System," 25 Nov. 2003.

[19] USAF/AEDC, "Tunnel 9 Completes Vehicle Testing," 1 Nov. 2005.

[20] Thompson, E., Henry, K., and Williams, L., "Guinness Recognizes NASA Scramjet," 20 June 2005.

[21] USAF, SR-71A Flight Manual (U), Oct. 1989, Change 2.

[22] Hicks, K. D., "Introduction to Astrodynamic Reentry," Air Force Institute of Technology, Wright–Patterson AFB, OH, Edition 0.7 (unpublished).

[23] Fogiel, M., *The Geometry Problem Solver*, Research and Education Association, NJ, 1977.

[24] Bryson, A. E., Jr., and Ho, Y.-C., *Applied Optimal Control*, Taylor and Francis, London, 1975.

[25] Athans, M., and Falb, P. L., *Optimal Control: An Introduction to the Theory and its Application*, Dover, New York, 2007.

[26] Clements, J. C., "Minimum-Time Turn Trajectories to Fly-To Points," *Optimal Control Applications and Methods*, Vol. 11, No. 1, 1990, pp. 39–50. doi:10.1002/oca.4660110104